Supplementary Information for "Origin of Low Electron-Hole Recombination Rate in Metal Halide Perovskites"

Francesco Ambrosio,*[a] Julia Wiktor,[a] Filippo De Angelis,[b,c] and Alfredo Pasquarello[a]

1 Computational details

We carry out molecular dynamics (MD) simulations at the hybrid functional level with the PBE0 functional[1,2] for the tetragonal $CH_3NH_3PbI_3$ in its ground state, and additionally for the system with an extra hole and an extra electron, respectively. The fraction of Fock exchange α is kept fixed at its original value (0.25). We include non-local van der Waals interactions through the rVV10 scheme.[3,4] All the calculations are performed with the CP2K suite of codes.[5] Goedecker-Teter-Hutter pseudopotentials are used to account for core-valence interactions.[6] We use double-ζ polarized basis sets for the wave functions[7] and a cut-off of 800 Ry for the expansion of the electron density in plane waves. We employ the auxiliary density matrix method with the cFIT auxiliary basis set.[8] We consider a 384-atoms supercell and take, as starting configuration, a structure with an apolar arrangement of the organic cations. The size of the employed supercell ($a = b = 17.72$ Å, $c = 25.32$ Å, corresponding to the experimental structure[9]) is of the same order as the localization of the band-edge states that was observed in Ref. 10. Therefore, the charge densities of the hole and the electron in the charged supercells are representative of realistic conditions. The target temperature for the MD runs in the NVT ensemble is set at 300 K and controlled by a Nosé-Hoover thermostat.[11,12] A time-step of 1 fs is employed and MD runs are carried out for 5 ps. The spin-orbit coupling effects on the localization properties are evaluated through semi-relativistic electronic-structure calculations on selected structures obtained from our MD simulations. In these calculations, we use a plane-wave basis set with an energy cut-off of 32 Ha and norm-conserving pseudopotentials for describing core-valence interactions,[13] as provided in the QUANTUM ESPRESSO package.[14]

To ensure that the calculations are not biased by the self-interaction error, we verified that the employed hybrid functional complies with the Koopmans' condition[15] for the material under investigation. To this end, we first employed the PBE0 functional with the fraction of Fock exchange α set to the standard value of 0.25, obtaining charge localization upon structural relaxation. Next, we kept the achieved structure fixed and determined the fraction α, for which the single-particle energy-level associated with the extra electron or the extra hole does not vary upon occupation, as required by exact density functional theory.[15] We obtain $\alpha = 0.22$ and $\alpha = 0.24$ for the electron and the hole, respectively. Hence, the use of $\alpha = 0.25$ guarantees that our calculations are essentially devoid of the self-interaction error.

2 Polaron binding energies

To calculate the energy levels for the model used in this work, we adopt the grand-canonical formulation of defects in crystalline materials.[16,17] In this formulation, the free energy of a defect $G^q_f[X]$ is expressed as a function of the electron chemical potential μ:

$$G^q_f[X] = G^q[X] - G[\text{bulk}] - \sum_i n_i\mu_i + q(\varepsilon_v + \mu), \quad (1)$$

where $G^q[X]$ is the free energy of the defect X in the charge state q, $E[\text{bulk}]$ is the free energy of the pristine bulk system, μ_i is the chemical potential of the subtracted/added species i, ε_v the valence band edge of the pristine system. Electrostatic finite size corrections can be neglected due to the large static dielectric constant of $CH_3NH_3PbI_3$ ($\varepsilon \sim 70$, from Ref. 18).

The charge transition level $\mu(q/q')$ is defined as the electron chemical potential for which the free energies of formation of a defect X in the charge states q and q' are equal, $\Delta G(q/q') = 0$.[16,17] This results in the following expression for $\mu(q/q')$:

$$\mu(q/q') = \frac{G^q[X] - G^{q'}[X]}{q' - q} - \varepsilon_v, \quad (2)$$

For the localization of the hole, we can write the following reaction:

$$CH_3NH_3PbI_3 + h^+ \rightarrow h_{loc} \quad (3)$$

The hole polaron level can then be defined as follows:

$$\mu(h_{loc}) = G[h_{loc}] - G[CH_3NH_3PbI_3] - \varepsilon_v, \quad (4)$$

where $G[h_{loc}]$ is the free energy of the localized hole and

[a] Chaire de Simulation à l'Echelle Atomique (CSEA), Ecole Polytechnique Fédérale de Lausanne (EPFL), CH-1015 Lausanne, Switzerland. E-mail: Francesco.Ambrosio@epfl.ch
[b] Computational Laboratory for Hybrid/Organic Photovoltaics (CLHYO), CNR-ISTM, Via Elce di Sotto 8, I-06123 Perugia, Italy.
[c] D3-Computation, Istituto Italiano di Tecnologia, Via Morego 30, Genova, Italy.

$G[CH_3NH_3PbI_3]$ that of the bulk perovskite. To account for the rotational degrees of freedom of the methylammonium cations within their Pb-I cages, we use the thermodynamic integration method [19] to calculate the free-energy difference in Eq. (4). Therefore, we introduce a fictitious Hamiltonian $\mathscr{H}_\eta$:

$$\mathscr{H}_\eta = \eta \mathscr{H}_{h_{\rm loc}} + (1-\eta)\mathscr{H}_{CH_3NH_3PbI_3}, \tag{5}$$

which connects the Hamiltonian of the reactant $CH_3NH_3PbI_3$ with that of the product $h_{\rm loc}$, via the Kirkwood coupling parameter η, which ranges from 0 to 1. [19] Hence, the free-energy difference appearing in Eq. (4) is given by: [19,20]

$$G[h_{\rm loc}] - G[CH_3NH_3PbI_3] = \int_0^1 \langle \Delta E_h \rangle_\eta d\eta, \tag{6}$$

where $\langle \Delta E_h \rangle_\eta$ correspond to vertical energy differences for structural configurations achieved at various values of η. In this work, we use the values of $\eta = 0$ and $\eta = 1$ to achieve a linear approximation for $\langle \Delta E_h \rangle_\eta$. For these values of η, $\langle \Delta E_h \rangle_0$ corresponds to the energy of vertical removal of one electron. $\langle \Delta E_h \rangle_1$ corresponds to the vertical reduction energy of $h_{\rm loc}$. In this way, the hole polaron level reads:

$$\mu(h_{\rm loc}) = \frac{\langle \Delta E_h \rangle_0 + \langle \Delta E_h \rangle_1}{2} - \varepsilon_{\rm v} \tag{7}$$

Analogously, we can write the following reaction for the extra electron:

$$CH_3NH_3PbI_3 + e^- \rightarrow e_{\rm loc}. \tag{8}$$

The respective charge transition level is then given by:

$$\mu(h_{\rm loc}) = \frac{\langle \Delta E_e \rangle_0 + \langle \Delta E_e \rangle_1}{2} - \varepsilon_{\rm v}, \tag{9}$$

where $\langle \Delta E_e \rangle_0$ is the energy associated with the vertical injection of an electron in $CH_3NH_3PbI_3$ and $\langle \Delta E_e \rangle_1$ the vertical binding energy of the localized electron $e_{\rm loc}$.

3 Hopping of charge localization

Figure S1 schematically illustrates the localization of the charge density in the inorganic sublattice during the molecular dynamics evolution of the extra hole and the extra electron. The extra hole is found to localize in planes orthogonal to the tetragonal axis and to hop from one plane to the other on a subpicosecond timescale [cf. Fig. S1(a)]. The extra electron modifies its local distribution on the same time scale, and its charge density is instantaneously found on Pb-I chains lying either parallel or perpendicular to the tetragonal axis [cf. Fig. S1(b)]. The high frequency of the observed changes in the localization ensures that the molecular dynamics simulation is sufficiently long to give a reliable representation of the observed phenomenon.

4 Inverse participation ratio in the excitonic state

In Fig. S2, $\langle \Psi_h | \Psi_e \rangle^2$ is displayed as a function of the average inverse participation ratio (IPR) of the wave functions of the hole and the electron in the excitonic state. The correlation between the extent of the localization and the overlap appears clearly. We also include in Fig. S2 the values calculated for structural configurations of the non-excited ground state in the presence of an excitonic excitation (red squares). We remark that the data points pertaining to the latter do not differ significantly from those achieved with the wave functions of the non-excited ground state (not shown). This allows us to emphasize the drop in $\langle \Psi_h | \Psi_e \rangle^2$ upon charge localization by approximately two orders of magnitude. In addition, Fig. S2 gives the values calculated for the orthorhombic phase and for the artificial system without dipolar field, referred to in the main text.

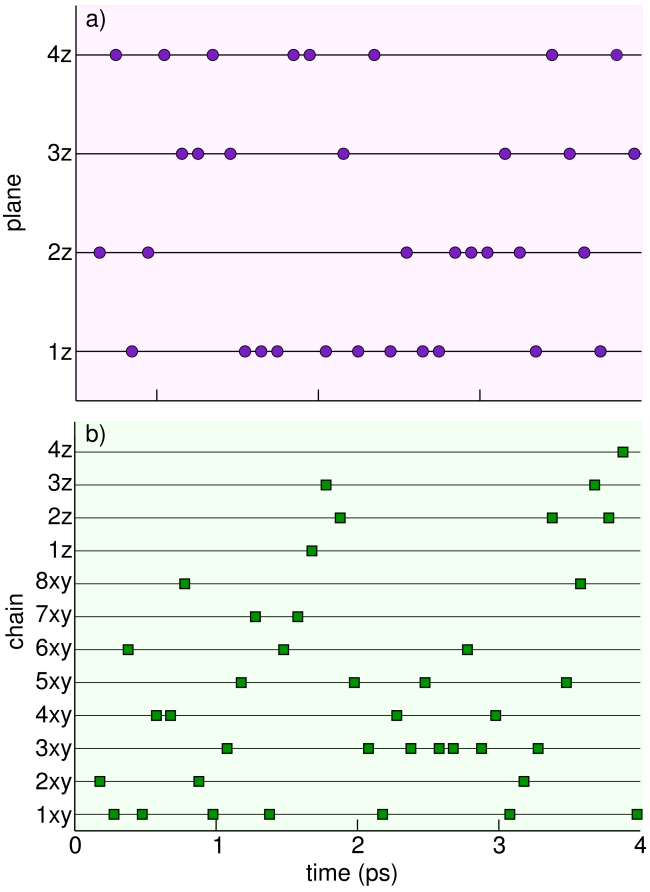

Fig. S1 Hopping of the charge localization during the molecular dynamics of the extra hole and the extra electron. (a) The hole density localizes in planes of the inorganic sublattice orthogonal to the tetragonal axis (labeled $1z$ to $4z$) and (b) the electron density in Pb-I chains either parallel (labeled $1xy$ to $8xy$) or orthogonal (labeled $1z$ to $4z$) to the tetragonal axis.

5 Correlation between the dipolar field of the organic cations and the charge localization

The role of the dipolar field associated with the organic cations in determining the localization of the charge density is demonstrated in Fig. S3. We focus on the molecular dynamics of the exciton and first take the hole density under consideration. For each considered snapshot, we identify the plane in which the positive charge density localizes. In Fig. S3(a), we show the distribution of distances of the C atoms of the adjacent organic cations to the instantaneously charged plane. Compared to the overall dis-

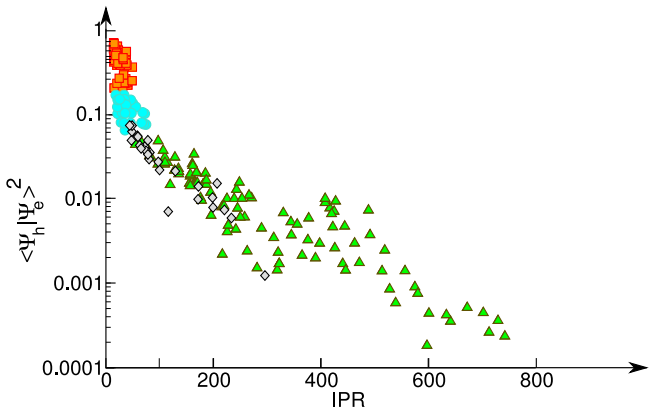

Fig. S2 $\langle\Psi_h|\Psi_e\rangle^2$ vs. the average of the IPR for the extra hole and the extra electron in the excitonic state (green triangles). Values calculated for the non-excited ground state (red squares), for the exciton state in the orthorhombic phase (blue circles) and in a artificial system, in which the organic cations are replaced with immobile Cs^+ ions at the cage centers (grey losanges), are also reported.

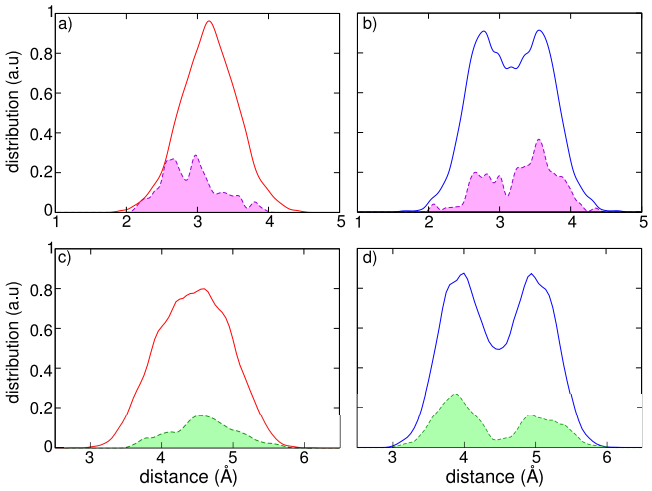

Fig. S3 Correlation between dipole orientation of the organic cations and charge localization. Panels (a) and (b) refer to the hole density in the molecular dynamics simulation of the exciton, and show the distances between the charged plane and the (a) C and (b) N atoms of adjacent organic cations, compared to their overall distributions (solid lines). Similarly, we focus in panels (c) and (d) on the electron density in the same dynamics. In this case, panels (c) and (d) represent the respective distances to the linear Pb-I chain, on which the electron charge density is localized.

tribution of C distances, i.e. without considering the location of the charge density, the C distances in the cations adjacent to the plane are found to be slightly biased towards the low-distance side. As the C atoms correspond to the negative poles of the dipolar organic cations, the identified orientation is consistent with the electrostatic attraction between the hole and the molecular dipole, and thus emphasizes the correlation between the dipolar field and the charge localization. In Fig. S3(b), we give the distances for the N atoms corresponding to the positive poles of the dipolar cations and find a preference for larger distances, as opposed to the behavior of the C atoms. The correlation between dipolar field and localization also applies to the electron density in the same simulation of the exciton. In this case, we focus on negative charge distributions that are localized on chains of Pb and I atoms. Figures S3(c) and (d) correspond to C and N distances to the charged linear chain, respectively. Hence, the bias is reversed with respect to the case of the extra hole, consistent with the localization of negative charge in the chains.

To further demonstrate that the localization of the extra hole and of the extra electron are associated with the orientation of the organic cations in their cages, we consider an instantaneous structure of $CH_3NH_3PbI_3$ taken from the evolution at 300 K of the neutral ground state, in which the organic cations show a given orientation. Then, we perform a structural relaxation upon adding an extra hole and observe hole localization, as shown in Fig. S4(a). Using the same ground-state structure, we add an extra electron and observe a different localization, as shown in Fig. S4(b). The structural relaxations performed here allow for small distortions of the inorganic sublattice, but do not lead to any reorientation of the organic cations. Next, we exchange the positions of the C and N atoms in the organic cations and obtain by structural relaxation a modified neutral structure, in which the orientations associated with the organic cations are reversed. Repeating the same operations as for the previous structure, we obtain the charge densities for the extra hole and the extra electron hole given in Figs. S4(c) and (d), respectively. We observe that the charge densities before and after inversion localize in different spatial regions, indicating that the dipole field of the organic cations plays a role in the charge localization. However, as shown in the main text, the localization is primarily induced by the thermal vibrations of the inorganic sublattice.

References

1 J. P. Perdew, M. Ernzerhof and K. Burke, *J. Chem. Phys.*, 1996, **105**, 9982–9985.

2 C. Adamo and V. Barone, *J. Chem. Phys.*, 1999, **110**, 6158–6170.

3 O. A. Vydrov and T. Van Voorhis, *J. Chem. Phys.*, 2010, **133**, 244103.

4 R. Sabatini, T. Gorni and S. de Gironcoli, *Phys. Rev. B*, 2013, **87**, 041108.

5 J. VandeVondele, M. Krack, F. Mohamed, M. Parrinello, T. Chassaing and J. Hutter, *Comput. Phys. Commun.*, 2005, **167**, 103 – 128.

6 S. Goedecker, M. Teter and J. Hutter, *Phys. Rev. B*, 1996, **54**, 1703–1710.

7 J. VandeVondele and J. Hutter, *J. Chem. Phys.*, 2007, **127**, 114105.

8 M. Guidon, J. Hutter and J. VandeVondele, *J. Chem. Theory Comput.*, 2010, **6**, 2348–2364.

9 Y. Kawamura, H. Mashiyama and K. Hasebe, *J. Phys. Soc. Jpn.*, 2002, **71**, 1694.

10 J. Ma and L.-W. Wang, *Nano Letters*, 2015, **15**, 248–253.

11 S. Nosé, *J. Chem. Phys.*, 1984, **81**, 511–519.

12 W. G. Hoover, *Phys. Rev. A*, 1985, **31**, 1695–1697.

13 D. Hamann, *Phys. Rev. B*, 2013, **88**, 085117.

14 P. Giannozzi, S. Baroni, N. Bonini, M. Calandra, R. Car,

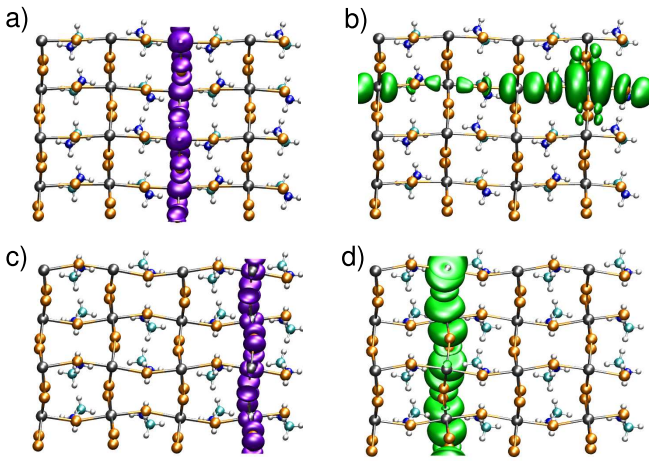

Fig. S4 Isodensity representations of an (a) extra hole and an (b) extra electron for a structure of $CH_3NH_3PbI_3$ with a given orientation of the organic cations. When the orientations of the organic cations are inverted, the respective charge densities change to (c) and (d). Pb atoms in grey, I in orange, C in cyan, N in blue, and H in white. The tetragonal axis lies horizontally.

C. Cavazzoni, D. Ceresoli, G. L. Chiarotti, M. Cococcioni, I. Dabo *et al.*, *J. Phys.: Condens. Matter*, 2009, **21**, 395502.

15 J. P. Perdew, R. G. Parr, M. Levy and J. L. Balduzi Jr., *Phys. Rev. Lett.*, 1982, **49**, 1691.

16 H.-P. Komsa, T. T. Rantala and A. Pasquarello, *Phys. Rev. B*, 2012, **86**, 045112.

17 C. Freysoldt, B. Grabowski, T. Hickel, J. Neugebauer, G. Kresse, A. Janotti and C. G. Van de Walle, *Rev. Mod. Phys.*, 2014, **86**, 253–305.

18 Q. Lin, A. Armin, R. C. R. Nagiri, P. L. Burn and P. Meredith, *Nature Photonics*, 2015, **9**, 106–112.

19 D. Frenkel and B. Smit, *Understanding Molecular Simulation: from Algorithms to Applications*, Academic Press, 2002.

20 F. Ambrosio, G. Miceli and A. Pasquarello, *J. Chem. Phys.*, 2015, **143**, 244508.